



How do drivers respond to driving risk during car-following? Risk-response driver model and its application in human-like longitudinal control

Xiaocong Zhao ^{a,b}, Ren He ^b, Jianqiang Wang ^{c,*}

^a College of Transportation Engineering & the Key Laboratory of Road and Traffic Engineering, Ministry of Education, Tongji University, Shanghai, 201804, China

^b School of Automotive and Traffic Engineering, Jiangsu University, Zhenjiang 212013, China

^c State Key Laboratory of Automotive Safety and Energy, Tsinghua University, Beijing 100084, China



ARTICLE INFO

Keywords:

Intelligent connected vehicle
Road safety
Driver modeling
Risk field theory
Car-following tasks
Human driving strategy

ABSTRACT

The blooming of intelligent connected vehicle (ICV) has been continuously shaping a hybrid traffic environment in which the road is shared among ICVs and vehicles driven by human drivers. However, due to the insufficient understanding of the human driving strategy and style, the conflicts between ICVs and human drivers have arisen public attention, threatening the road safety and bottlenecking the development of ICV. In order to embed the human driving strategy in the intelligent driving system, researchers have been rolling out efforts on driver modeling. Most driver models, however, still suffer from the limited application scope or poor transparency. Within our finite horizons, a unified and readable driver model for various driving scenarios is generally unobtainable. In this work, we tried to model the human driving strategy from an aspect of human nature, that is, the way human drivers respond to the driving risk. We employed the risk field theory (also known as the safety field theory) to model the environmental risk in a comprehensive manner. By studying the risk-response strategy from the driving data of 24 human drivers, we proposed a unified structure, which we call the risk-response driver model (RRDM), to model the human driving strategy. This model provides access to learning not only the average driving strategy of a group of human drivers but also the specific driving style of a single driver. The explicit and readable driving strategy produced by RRDM can be directly employed to reproduce human-like longitudinal driving control. We verified the performance of our model in car-following tasks and found that its human-like driving performance is recoverable among the human drivers who participated in the tests.

1. Introduction

Emerging technologies of intelligent connected vehicles (ICVs) have been continuously shaping the foreseeable vehicular traffic into a hybrid one in which the road is shared among human drivers, man-machine shared driving, and fully automated vehicles (Rahman et al., 2018). Being new in the road traffic, ICVs need to mimic the human driver mechanism in order for them to potentiate acceptance from the society (Gu et al., 2017; Hecker et al., 2019; Marina Martinez et al., 2018). As such, driver modeling plays an indispensable role in the mimicking of a human driver. Herein, we define the modeling of a human driver as a process of formulating a human driving strategy, which is an inherent rule when defining how a driver should respond to given stimuli in specific scenarios through the conduction of driving maneuvers (Benderius, 2012). Fig. 1 shows the driver model, which mainly comprises three components: (1) the model input extracted from the

environmental and vehicular dynamics, namely, the stimuli; (2) the model parameters that reflect how a driver model would react to different stimuli, namely, the driving style; and (3) the model output produced through mimicking a human driving strategy, namely, the response. Of these components, the driver model response usually includes acceleration, braking, and steering, whereas the selection of the model input and the method for individualizing model parameters varied in previous works.

Selection of Model Input. When designing a contemporary driver model, a specific driving scenario is usually considered. Thus, depending on the scenario being studied, researchers may purposely select environmental information as the model input. A vital and fundamental example can be the car-following scenario (Cao, 2020; Liu et al., 2020). Conventional car-following models, including General Motors based model (GM) (Chakraborty and Kikuchi, 1999), intelligent driver model (IDM) (Treiber et al., 2000), etc., pay special attention to longitudinal

* Corresponding author.

E-mail address: wjqlws@tsinghua.edu.cn (J. Wang).

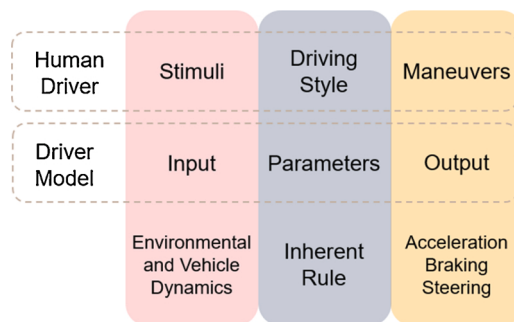


Fig. 1. Relationship between human driver and driver model.

measures like longitudinal position, spacing, relative speed, time to collision (TTC), and the like. With the blooming ICV, researchers have developed numerous modern applications for the human-like automated vehicle control based on these conventional models. For example, an enhanced and widely used version of IDM was presented by Kesting et al. (2010) which relieved the hard braking problem in the original version. Many subsequent works focusing on the longitudinal control of ICV have been carried out based on this landmark model (Li et al., 2015; Goodall and Lan, 2020). Aside from modification-based works, Wang et al. (2013) analyzed statistical features of time headway (THW) and TTC in human driving data and presented a driver model, employing THW and TTC as inputs. Marzbanrad and Moghaddam (2016) proposed a longitudinal control method that mainly employs the relative distance as the model input. As such, most models limited the inputting measures in the longitudinal dimension for the practicality. However, from the perspective of microscopic driving behavior modeling, these conventional models usually suffer from the fact that real-world driving scenarios are far more complex. For instance, the cut-in maneuver of an adjacent vehicle is an inevitable and commonly mentioned challenge for longitudinal vehicle control (Milanes and Shladover, 2016). This is because the cut-in event is usually considered a lateral risk by a human driver, while for a single-dimensional car-following model, this event is detected as a sudden change in longitudinal measures, which is unfavorable to the control. To address this problem, (Liu et al., 2017) developed a virtual lead vehicle scheme in simulation by taking lateral interruptions (cutting in/out events) into account. More recent research by Fu et al. (2019) conducted on-road tests and provided a car-following model considering the cut-in behaviors of surrounding vehicles. However, the fitting-based method in this work limited its potential generalization in other scenarios.

Individualization of Model Parameters. The parameters of a driver model are supposed to capture the human aspects (Macadam, 2003), which are usually known as the driving style. In most cases, these parameters are obtained through a training process, during which they are adjusted to let the model output operations in a manner that is as close as possible to what human drivers do (Kuderer et al., 2015; Xu et al., 2015). To date, in consideration of the various characteristics of human drivers, there have been substantial efforts rolling out in order to represent human diversity in driver models. One popular method for shaping different driving styles is discrete classification. The design of classification-based models usually cover three steps, as follows: (1) construction of a driving feature vector that includes scenario dynamics (speed, spacing, and relative speed, etc.) and driving maneuvers (acceleration, braking, and steering) (Wilson, 2008); (2) based on the driving feature vector, classifying human drivers into discrete types using unsupervised clustering or according to a self-defined criterion (aggressive /medium(normal) /calm(cautious)) (Constantinescu et al., 2010; Xu et al., 2015; Zhu et al., 2019); and (3) training the driver models for each driver group. Admittedly, through classification, one can obtain a set of driver models that follow different driving styles. However, driving styles distinguished by indicators like aggressiveness

remain ambiguous. For example, assuming three driver models that are labeled as aggressive, medium, and calm, respectively, we will still find it hard to decide which one should we prefer for autonomous driving. One may claim that the “calm” type is ideal in terms of safety; however, there will be instances in which “aggressive” maneuvers defined by model designers are imperative (McCall and Trivedi, 2007). Moreover, although as a whole the parameter vector, to some extent, represents a driving style, each parameter alone usually does not stand for any explicit feature of the driving strategy. As such, there remains vagueness from which the tuning process may suffer.

Likewise, continuous indexing of a driving style has been applied in the longitudinal control model (LCM) presented by Ni et al. (2015). LCM employs two parameters—the estimate of the emergency deceleration most likely to be applied by the leading car and the deceleration at which the driver in an ego car believes is applicable in the situation—to measure the aggressiveness of the human driver. Theoretically, we can obtain a well-individualized driver model to mimic any single driver by tuning the parameters. With the bloom of artificial intelligence technology, the learning-based stimuli-response driver model (Benderius, 2012; Bojarski et al., 2016; Pathak et al., 2019; Xu et al., 2015) has been proven to extract stimuli with high completeness from environmental dynamics and possibly provide a better interpretation to the human-like driving. However, apart from poor transparency, the robustness of end-to-end methods depends excessively on high-quality training data.

In summary, (a) driver models in most studies are application-driven and scenario-dependent. A unified structure for driver modeling is still lacking and (b) an interpretable and intuitive driver model design is needed to serve the explicit model tuning.

In this work, we propose a unified structure for driver modeling from the perspective of learning the way human drivers respond to traffic risks. Based on the risk field theory (Wang et al., 2014, 2015, 2016), the environmental and vehicular dynamics are unified to form the model input, which is the risk. Accordingly, we propose a risk-response driver model (RRDM) to explain the human driving strategy in the car-following task in an explicit way.

There are three main contributions of this work, as follows:

- (1) Proposal of a novel paradigm for modeling human driver by learning the way human drivers respond to the driving risk.
- (2) Proposal of an intuitive and readable driver model for the car-following task, the RRDM, in which the model parameters could numerically reveal the driving style in the training data.
- (3) Design of an RRDM-based exemplary application for human-like longitudinal control and verification of its performance in simulations, under GM and IDM benchmarks.

2. Data collection

2.1. Experimental setup

In order to collect human driving data, we used a Honda Accord sedan (Vehicle A) and two Changan Yuexiang sedans (Vehicles B and C). Fig. 2 shows the devices that were equipped on the three experimental vehicles. A wireless safety unit was used to realize vehicle-to-vehicle (V2V) communication among experimental vehicles. Moreover, an on-board industrial computer (OIC) was used to collect the position data and controller area network (CAN) data recorded using the global positioning system and the CAN bus, respectively. The collected data from all three vehicles were then synchronized and labeled with timestamps.

2.2. Drivers and driving scenarios

24 licensed drivers (20 males, four females) participated in the road experiments. The average age of the drivers and the average driving experience were 36.5 years [standard deviation (SD) = 9.6 years] and 11

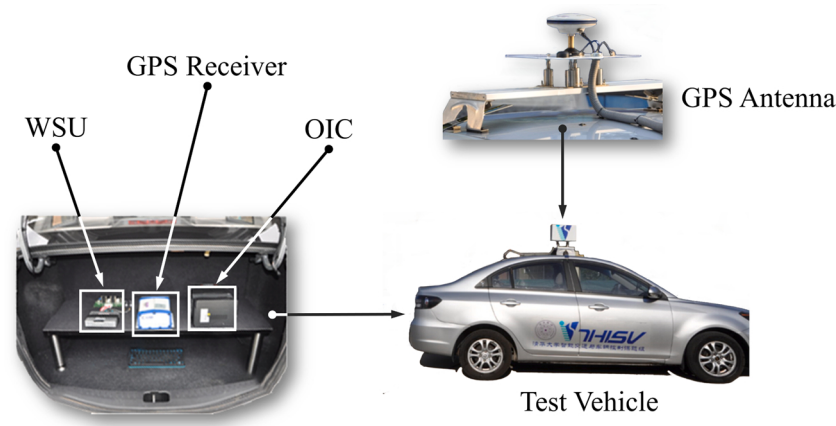


Fig. 2. Experimental setup.

years ($SD = 6.9$ years), respectively. The participant drivers were company employees, university faculty, and freelancers; there were no professional drivers among them.

The testing route was a 3 km long segment of Shuinan Road in the district of Changping in Beijing, China. The participant drivers were

Algorithm 1. Speed Control.

Input	$n, t, T, T_set = \{(24,36), (30,30), (32,28), (25,35), (34,26), (27,33)\}$
Output	v_A
1	For $n = 1:6$
2	Read the period set: $T_set(n)$
3	Select a period randomly from period set: $T = \text{random}(T_set(1), 1)$
4	For $t = 1:T$
5	Calculate the target speed of vehicle A: $v_A = 45 + 20 \sin(2\pi t/T)$ (km/h)
6	End for
7	If $n = 6$
8	Reset $n = 1$
9	End if
10	End for

instructed to complete a round-trip journey in each scenario, which makes a total distance of 6 km. There were two driving scenarios in the road experiments, namely, pure car-following and compound car-following.

- (1) Pure Car-Following Scenario. In this scenario, only Vehicles A and B were involved, as shown in Fig. 3(a). Here, the participant drivers were asked to drive Vehicle B and follow Vehicle A.
- (2) Compound Car-Following Scenario. Here, the participant drivers were instructed to maintain the car-following activity, as indicated in Fig. 3(b). In addition, a skilled driving tester was instructed to drive Vehicle C in the adjacent lane and to randomly conduct four cut-in maneuvers and nine attempts to cut in for each round trip.

2.3. Additional details

- (1) The speed of vehicle A is automatically controlled by Algorithm 1. The speed changes periodically, and the period T (s), which ranges between [24, 36] and changes after every period, was randomly selected in given sets. Fig. 4 shows the speed of vehicle A during a whole test trip.
- (2) Except for the test vehicles, the volume of other vehicles is neglectable.

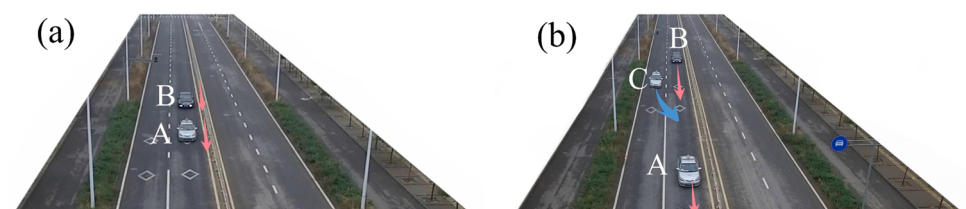


Fig. 3. Experimental scenarios: (a) Pure car-following; (b) Compound car-following.

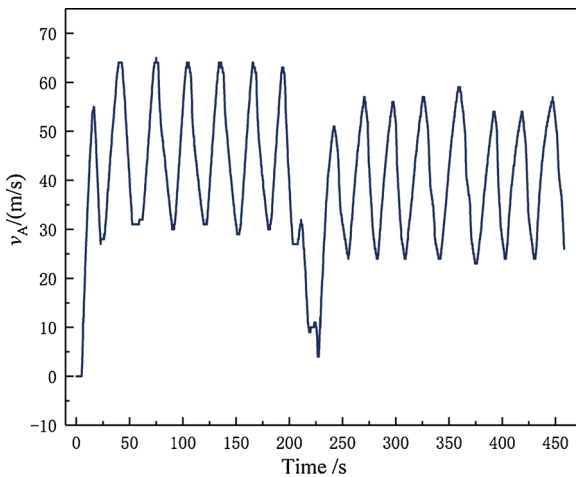


Fig. 4. Speed of vehicle A during a round trip.

3. A modified driving risk field model

In order to describe the driving risk in a unified manner, we employed the risk field theory, which we have proposed in our previous work. The risk field model describes the risk associated with various traffic factors based on human-vehicle-road interaction. A well-rounded introduction of the risk field theory is presented in works by Wang et al. (2015). Nonetheless, for the application of this study, we streamlined the risk field model for the specific scenarios covered in road experiments. Note that the driving risk field model that we have presented in this paper can be extended to more complex driving scenarios.

3.1. General structure

Surrounding traffic units mainly create driving risks. By this principle, we can define each surrounding unit to be a source of risk, which interacts with the subject vehicle by forming a risk field. The risk field strength of a traffic unit can be expressed as

$$E_{ij} = D_{ij} \cdot R_i \quad (1)$$

where E_{ij} is the *field strength* vector of the traffic unit i at position j , pointing from i to j ; D_{ij} is the *field distribution* vector of the traffic unit i at position j , pointing from i to j , which denotes the spatial features of risk distribution; and R_i is the *risk volume* of unit i , which denotes the magnitude of the risk emitted by the traffic unit i . Detailed modeling of *risk volume* and *field distribution* is presented in the subsequent texts on model design.

3.2. Rule-based model design

In order to fulfill human-like risk perception, the *risk volume* and the *field distribution* of our modified risk field model follow four straightforward rules. Briefly, four rules have been listed in Table 1, and details

Table 1

Design rules of modified driving risk field model.

	Description	Affected Components
Rule 1	The risk volume of a traffic unit depends on its properties and motion state.	<i>Risk Volume</i>
Rule 2	Risk decreases with the distance to a risk source.	
Rule 3	The driving risk is greatest at the front of an approaching object.	<i>Field Distribution</i>
Rule 4	Traffic markers and facilities constrain the risk.	

are discussed as follows.

3.2.1. Risk volume

Road traffic accidents are mainly collisions between traffic units. During a collision, the kinetic energy of the units is released by extrusion and crushing, causing plastic deformation and other chain effects, which is usually denoted as “loss”. As depicted in **Rule 1**, the potential severity of a collision accident mainly depends on the type, mass, and shape of the involved units. For moving units, the kinetic energy is also considered. Hence, the *risk volume* of a traffic unit can be expressed as

$$R_i = m_i \cdot \left(1 + k_1 |v_i|^2\right) \cdot T_{\text{shape}} \cdot T_{\text{type}} \quad (2)$$

where m_i and v_i are the mass and velocity of the traffic unit i , respectively; $k_1 = 0.1$ is an empirically defined constant; and $T_{\text{shape}} \in (0, 1)$ and $T_{\text{type}} \geq 1$ are the shape factor and the cargo factor, respectively. Here, the larger the value of T_{shape} , the more aggressive the shape of the traffic unit. Some vehicular units multiply their threat to road traffic with respect to the type of cargo that they transport. For example, the severity of an accident may increase owing to the leakage of hazardous cargo from tank trucks, hazardous gas/liquid transport vehicles, and the like. Thus, the larger the value of T_{type} , the higher the hazard level of the cargo of vehicular units. For nonvehicular units, T_{type} is fixed to 1.

3.2.2. Field distribution

Firstly, as stated in **Rule 2**, the larger the distance from a risk source, the weaker the perceived risk. This provides the most intuitive feature of risk distribution [Fig. 5(a)], which could be depicted by the distance-based distribution D_{ij}^* :

$$D_{ij}^* = \frac{1}{|r_{ij}|^\lambda} p_{ij} \quad (3)$$

Where $p_{ij} = r_{ij}/|r_{ij}|$ is the *direction* vector and r_{ij} is the *distance* vector, pointing from unit i to unit j . The constant λ is greater than zero. In particular, λ is decisive to the falling gradient and effective range of the risk distribution. As such, a greater λ indicates a sharper falling trend of the risk with the distance to the risk source and a smaller effective range of the risk radiation. In this study, we have empirically fixed the value of λ to 1.5.

Secondly, because of the limited ability to perceive higher derivative information (Macadam, 2003), human drivers conduct maneuvers mainly on the basis of spacing and its changing trend, which we refer to here as relative speed. Spacing information has been considered in **Rule 2**. Further, **Rule 3** takes into account the changing trend by the motion-based distribution D_i^{motion} [Fig. 5(a)]:

$$D_i^{\text{motion}} = \exp(|v_i - v_j| \cdot \cos(\theta)) \quad (4)$$

where $\theta \leq 180^\circ$ indicates the angle between the *relative velocity* vector $v_i - v_j$ and the *direction* vector p_{ij} .

Finally, traffic markers and facilities set the rules in road traffic for the purpose of maintaining road safety and traffic efficiency. Therefore, as described in **Rule 4**, the spatial distribution of the risk field is constrained because drivers are supposed to follow the traffic rules. Herein, we take the lane markers as an example to bring this into the light.

During a driving process, the risk associated with the leading car is not likely to be the same as that from a car in the adjacent lane (Wang et al., 2016), mainly because lane markers limit the lateral movement of the vehicles. When separated by a dashed line, a vehicle is not supposed to cross the lane without observing a proper gap; hence, we can say that the risk from the vehicle in the adjacent lane has been constrained. Otherwise, when separated by a solid line, a vehicle is not supposed to cross the lane deliberately under any circumstances; hence, we can say that the risk from the vehicle in the adjacent lane has been cut off. In either case, lane markers play the role of risk filters. Fig. 5(b)

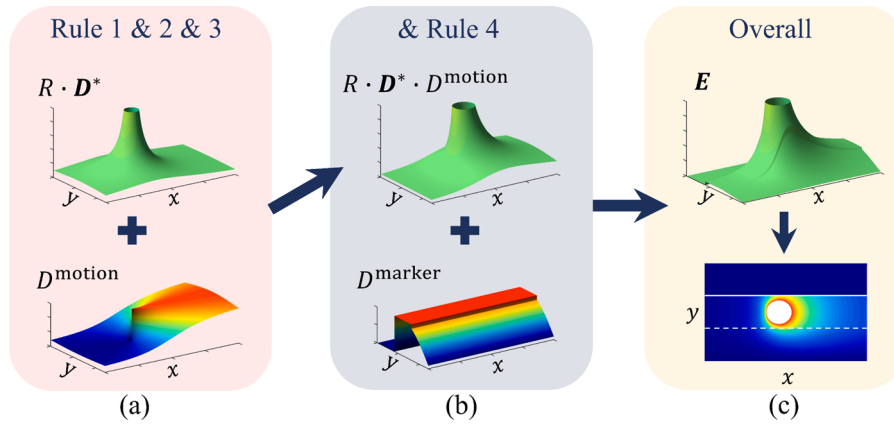


Fig. 5. Modified driving risk field model.

demonstrates the filtering effect, which could be mathematically expressed as D_j^{marker} :

$$D_j^{\text{marker}} = \begin{cases} T_{\text{marker}} \cdot \cos\left(|r_{j-lc}| \cdot \frac{\pi}{3w^*}\right) & |r_{j-lc}| > \frac{w^*}{2} \\ 1 & |r_{j-lc}| < \frac{w^*}{2} \end{cases} \quad (5)$$

where T_{marker} indicates the lane marker type. Herein, the value of T_{marker} for the solid line and the dashed line is 0 and 1, respectively. Moreover, the term r_{j-lc} is the vector pointing from the point j to the lane center, and w^* is the lane width.

Using Eq. (1) through (5), we obtained the overall field strength vector E_{ij} [Fig. 5(c)]:

$$\begin{aligned} E_{ij} &= D_{ij} \cdot R_i \\ &= (D_{ij}^* \cdot D_i^{\text{motion}} \cdot D_j^{\text{marker}}) \cdot R_i \end{aligned} \quad (6)$$

3.3. Interfield mechanism and risk effect

In a binary interaction, two units are mutually affected by the fields that they both generate. This interaction is usually achieved using force as a medium in the physics field. For example, when entities a and b are charged, the electric field force generated by object a to b and the effect of the electric field force on b can be described by Eq. (7) and (8), respectively:

$$\mathbf{F}_{ab}^e = E_{ab}^e \cdot Q_b \quad (7)$$

$$\mathbf{a}_b = \frac{\mathbf{F}_{ab}^e \cdot Q_b}{M_b} \quad (8)$$

where E_{ab}^e measures the electric field strength of entity a at the position of b , Q_b is the amount of charge of entity b , and M_b is the mass of entity b . Eq. (8) indicates that the effect of the electric field force is reflected on entity b in the form of acceleration, which is proportional to the amount of charge of b and inversely proportional to its mass.

Similarly, the interaction in driving risk field could be considered as a virtual force, which we here call the risk field force. This risk field force causes the object that it acts on to exhibit a tendency to move toward a low-risk position. According to this analysis, we can define the risk field force and risk effect as follows:

$$\mathbf{F}_j = \sum_{i=1}^n E_{ij} \cdot R_j \quad (9)$$

$$a_j^R = \frac{\mathbf{F}_j}{V_j} = \frac{\sum_{i=1}^n E_{ij} \cdot R_j}{V_j} \quad (10)$$

where \mathbf{F}_j is the risk field force generated by surrounding units to unit j , a_j^R is the risk effect on unit j ; n is the number of surrounding traffic units, and V_j is the resistance equivalent of unit j (to be discussed later). Eq. (9) posits that, given the location of units j and i , the larger the risk volume of unit j , the greater the risk field force acting on unit j . Similarly, Eq. (10) indicates that, given the risk field force acting on unit j , the larger the resistance equivalent of unit j , the weaker the risk effect. As such, the resistance equivalent is an index that determines how great a traffic unit may suffer once a collision is encountered. It is determined by the following equation:

$$V_j = (T_j \cdot F_{ij} \cdot V(x_j, y_j))^{-1} \quad (11)$$

where T_j is the index of the value type, F_{ij} is the index of vulnerability, and $V(x_j, y_j)$ is the spatial value distribution function. Essentially, T_j represents the overall value of the traffic unit j (the value type index of a human is larger than that of an empty car), F_{ij} represents how easily unit j could be damaged (the vulnerability index of a human is greater than that of a car), and $V(x_j, y_j)$ characterizes the distribution of the unit value over its volume range (for a manned car, the parts near the driver are considered more valuable).

4. Risk-response driver model

In order to fully understand how human drivers respond to risks, we

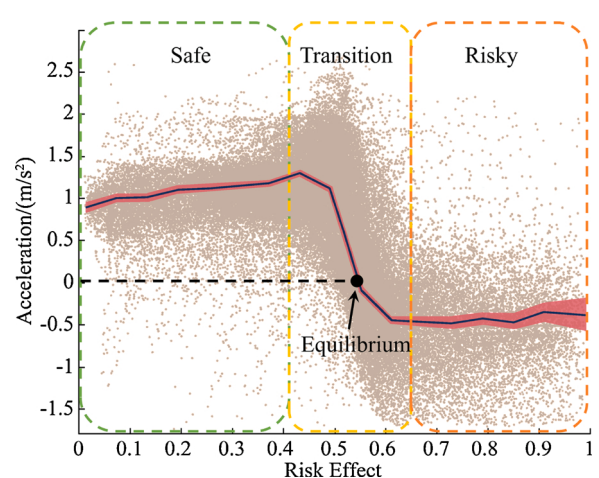


Fig. 6. Risk-response point cloud in driving data. The risk effect is normalized using min-max normalization. The curve indicates the mean value, and the shaded region indicates a 99.5 % confidence interval calculated using a t distribution.

analyzed the risk-response strategy of drivers in our dataset. We extracted a total of 102,994 valid frames, of which 53,330 frames were from the pure car-following scenario and 49,614 frames were from the compound car-following scenario. For each frame, we quantified the risk effect (a^R) of the subject vehicle (Vehicle B) using the risk field model that we have proposed in Section 3. Driving acceleration (a^D) was applied as the response of the human driver. The point cloud of longitudinal risk acceleration in all driving frames is captured in Fig. 6. Accordingly, we could observe gentle acceleration when the drivers are situated in a relatively low-risk level, which we have labeled as the safe range. There was a switch of driving maneuver from an acceleration mode to a braking mode during the transition range, and then the brake strength plateaued in more risky circumstances, which we call here the risky range. Fig. 6 also captures the mean value of acceleration and a 99.5 % confidence interval. Drivers' response was relatively stable in both the safe and the risky ranges, even after the risk level varied, which indicates that human drivers do not apply excessive acceleration in a thoroughly safe condition and, additionally, do not apply excessive braking in a highly dangerous situation. This phenomenon could be attributed to both the physical limits of the vehicles and the driving strategy of the human driver. Furthermore, within the transition range, we could observe an equilibrium, in which the driver demonstrated a tendency to maintain the risk level with cruising speed.

With respect to the risk-response features depicted in Fig. 6, we chose the S-curve (Fig. 7) to model the risk-response strategy of a human driver. Accordingly, our specific RRDM is defined as follows:

$$a_j^D = f^{\mathbf{P}_j}(\mathbf{a}_j^R) = (a_j^{\max} - a_j^{\min}) \frac{1}{1 + \exp(S_j \cdot (|\mathbf{a}_j^R| - M_j))} + a_j^{\min} \quad (12)$$

where $\mathbf{P}_j = [a_j^{\max} \ a_j^{\min} \ M_j \ S_j]^T$ is the parameter vector. The four parameters in RRDM reveal four characteristics of human drivers. The first two parameters, a_j^{\max} and a_j^{\min} , represent, respectively, the average value of maximum acceleration and the braking strength that driver j tends to apply. S_j is the factor of risk sensitivity: the greater its value, the smaller the transition range. In addition, a driver possessing high risk sensitivity can frequently switch between acceleration and braking when there is an intensive change in driving risk. Lastly, M_j is the risk equilibrium: a driver tends to maintain the driving risk around his/her risk equilibrium.

We utilized Eq. (12) to model the risk-response strategy of driver j , by finding the parameter vector $\hat{\mathbf{P}}_j$, which most precisely described his/her driving style. The parameter identification problem is formulated as:

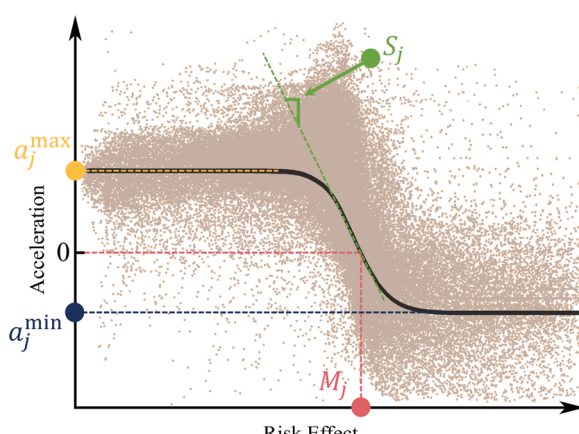


Fig. 7. Risk-Response curve of tested driver group.

$$\min_{\hat{\mathbf{P}}_j} \sum_{t=1}^{T_j} \left\{ f^{\hat{\mathbf{P}}_j} \left[\mathbf{a}_j^R(t) \right] - \mathbf{a}_j^D(t) \right\}^2 \text{ s.t. } \begin{cases} \hat{\mathbf{P}}_j \in \mathbb{R}^4 \\ a_j^{\max} \in (0, a_v^{\max}] \\ a_j^{\min} \in [-b_v^{\min}, 0) \\ T_j > 0 \end{cases} \quad (13)$$

where a_v^{\max} and b_v^{\min} are the maximum possible acceleration and deceleration, respectively, that could be conducted given the vehicle physics and T_j is the number of data frames collected from driver j .

Furthermore, we applied the particle swarm optimization (PSO) algorithm to identify the parameter vector of each driver. PSO algorithm is described in detail in (Wang et al., 2018). Table 2 lists all settings of the PSO algorithm for our present study.

We trained the parameter vector $\hat{\mathbf{P}}_j$ of each driver using his/her driving data in the first half of the round trip in the two testing scenarios*; the second half was remained for verification. By employing Eq. (12), we ensured that the driving strategy described by RRDM was transparent enough to shape an individualized human-like longitudinal control algorithm. We tested the performance of RRDM in longitudinal control in simulation, with respect to the following settings.

Pure Car-Following Scenario. For each driver, the temporal information of Vehicle A was reloaded so that a leading car was formed in the simulation. The RRDM of the relevant driver was applied to control Vehicle B and to deal with the car-following task given the same original spacing and velocity as those in real-world experiments.

Compound Car-Following Scenario. A total of 45 cut-in activities, starting from 5 s prior to any cut-in maneuver and lasting for at least 35 s, were manually extracted from the data for verification. For each cut-in activity, the temporal information of Vehicles A and C in real-world driving was reloaded so that a leading car and an adjacent car were formed in the simulation. The RRDM of the relevant driver was applied to control Vehicle B and to deal with both car-following tasks and cut-in events given the same original spacing and velocity as those in real-world experiments.

Altogether, a total of 69 travels were simulated in the two scenarios. For each travel, the IDM defined in Eq. (14) and the GM expressed in Eq. (16) were also applied to set the benchmark of the driving style. Table 3 provides a list of our model settings for IDM and GM in this work.

IDM. Consider the following equation:

$$a(t) = a_{\max} \left[1 - \left(\frac{v(t)}{\tilde{v}(t)} \right)^{\beta} - \left(\frac{\tilde{s}(t)}{s(t)} \right)^2 \right] \quad (14)$$

Here, a_{\max} represents the maximum acceleration of the following vehicle; \tilde{v} is the desired speed; \tilde{s} is the desired following spacing; v and s are the current speed and spacing, respectively; and β is a constant. Note that the desired spacing is a function of current speed (v), relative speed

Table 2
Settings of the PSO algorithm.

PSO Parameter	Value
Particle number	50
Maximal iteration number	100
Inertia weights	$0.5 + 0.4 \times \frac{\text{iter}}{100}$ (iter denotes the iteration step)
Speeding factor	1.5

* The data of driver #11 in the compound car-following scenario was lost because of sensor error; hence, only the data in pure car-following scenario was used for this driver.

Table 3
Settings of model benchmarks.

Model	Parameter	Value (unit)
IDM	Desired speed, \bar{v}	120 (km/h)
	Constant, β	5
	Maximum acceleration, a_{\max}	7 (m/s^2)
	Comfortable deceleration, a_{comf}	2 (m/s^2)
	Minimum spacing at a standstill, s_0	2 (m)
	Desired time headway, \tilde{T}	1.5 (s)

(Δv), maximum acceleration (a_{\max}), comfortable acceleration (a_{comf}), minimum spacing at a standstill (s_0), and desired time headway (\tilde{T}). Mathematically, we can express \tilde{s} as

$$\tilde{s}(t) = s_0 + \max \left(0, v(t)\tilde{T} - \frac{v(t)\Delta v(t)}{2\sqrt{a_{\max}a_{\text{comf}}}} \right) \quad (15)$$

GM. Consider the following equation:

$$a(t) = \alpha \frac{v(t)\Delta v(t)}{s(t)} \quad (16)$$

Here, v and s represent the current speed and spacing, respectively; Δv is the relative speed, and α is a constant.

5. Results

5.1. Individualized driving style

Fig. 8 presents a graphical distribution of the identified parameters of RRDM for the participant drivers. Shapiro-Wilk tests on these identified parameters were not significant ($\alpha = 0.01$), which indicates that the four parameters generally demonstrated a normal distribution. The result is consistent with the random selection of the participant drivers. As such, in Fig. 8, we analyzed the correlations between every two parameters of the RRDM. Only M_j and S_j showed a negative correlation coefficient of -0.59 . Apart from M_j and S_j , there was no significant correlation in any other parameter combination at a significance level of 0.05. Further, as the parameter vector denotes the driving style of the RRDM, we used a style map (Fig. 9) to illustrate the features in driving styles, which were abstracted from the driving data of each participant driver.

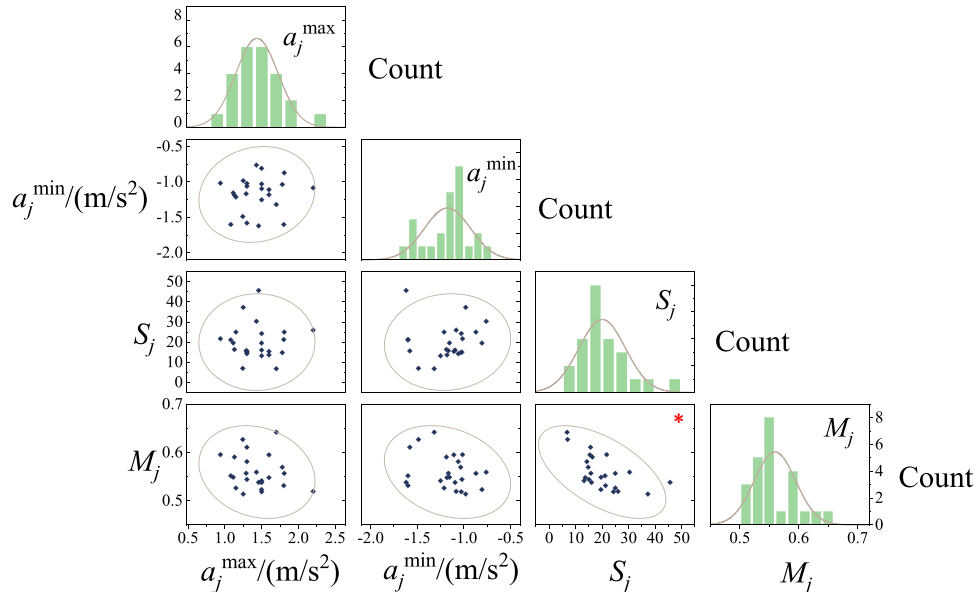


Fig. 8. Correlation matrix of four driver features in the RRDM. The asterisk (*) indicates that the correlation is significant at the 0.05 level (two-tailed).

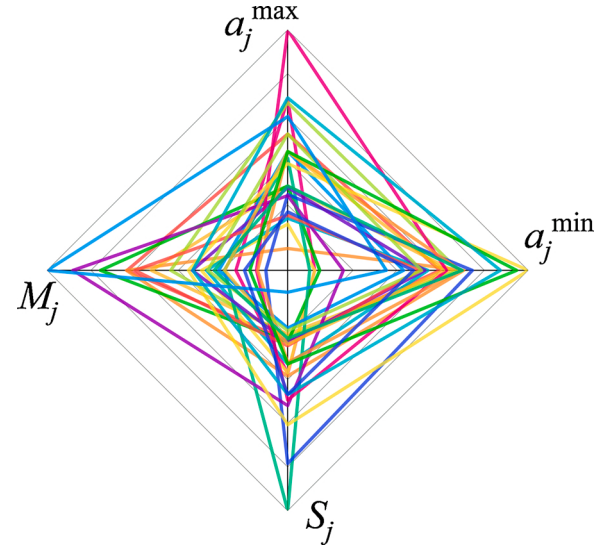


Fig. 9. Style maps of the participant drivers. Parameters are normalized using min-max normalization. Parameters obtained from a specific human driver are connected.

5.2. Performance of the RRDM in longitudinal control

As mentioned in the earlier sections, our purpose of this study covers revealing the inherent driving strategy of the human driver. As such, we have chosen the RRDM of three typical drivers in our dataset to analyze the performance of RRDM in dealing with a driving task in two experimental scenarios. Here, RRDM_j was used to denote the RRDM that has been trained with the data from driver #j.

5.2.1. A. Pure car-following scenario

Fig. 10 illustrates the driving process of driver #16 in the pure car-following scenario. RRDM₁₆ was defined by a parameter vector $\mathbf{P}_{16} = [a_{16}^{\max} = 1.50; a_{16}^{\min} = -1.03; M_{16} = 0.52; S_{16} = 19.32]^T$, and its driving style map is shown in Fig. 11. This driver maintained a low risk level by keeping relatively long spacing (mean: 36.62 m, SD = 13.65 m) from the leading car. This driving strategy was mainly characterized by RRDM₁₆ with a low risk equilibrium $M_{16} = 0.52$ (the average risk equilibrium of

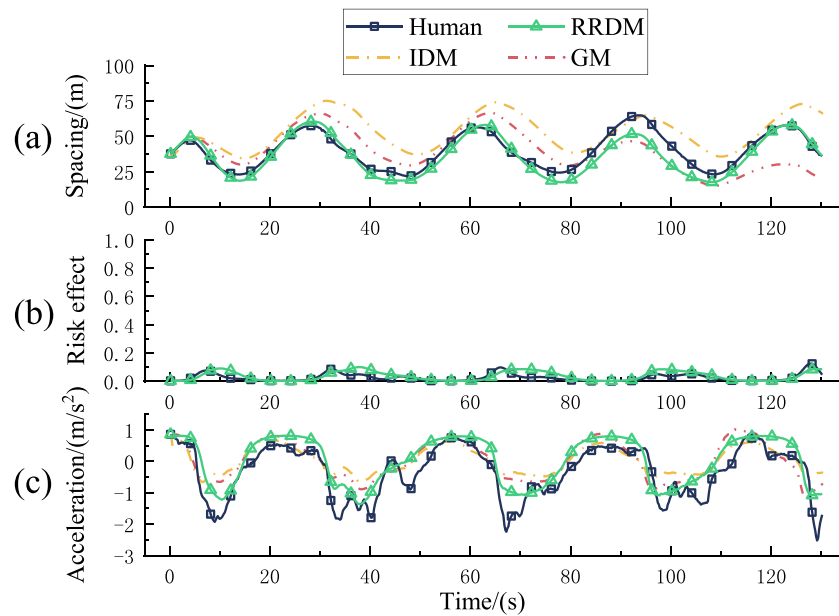


Fig. 10. Driving process of #16 driver in a pure car-following scenario.

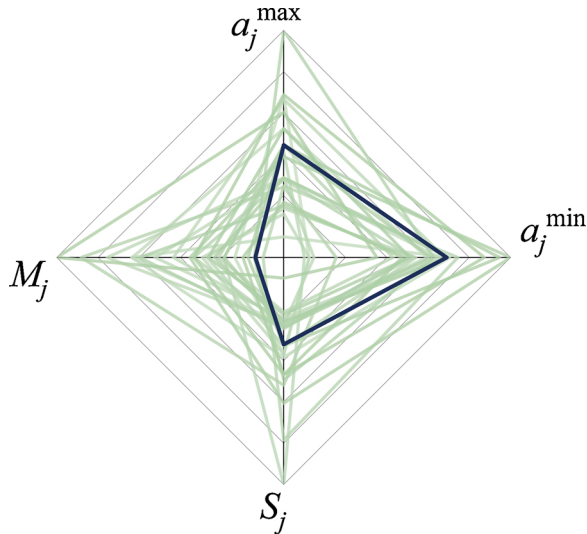


Fig. 11. Style map of driver #16.

the participant drivers was 0.56). The average spacing controlled by RRDM_{16} was shorter than that controlled by the IDM (mean: 53.29 m, SD = 12.25 m) and the GM (mean: 41.90 m, SD = 13.79 m), whereas the SD of spacing controlled by RRDM_{16} was between that controlled by the GM and that controlled by the IDM. Compared with the two baseline models, the spacing control strategy of RRDM_{16} is consistent with that of human driver #16 (mean: 40.01 m, SD = 12.33 m).

Accordingly, Fig. 12 describes the driving process of driver #13 in the car-following scenario. RRDM_{13} was defined by a parameter vector $\mathbf{P}_{13} = [a_{13}^{\max} = 1.24; a_{13}^{\min} = -1.49; M_{13} = 0.63; S_{13} = 26.98]^T$, and its driving style map is shown in Fig. 13. In contrast to driver #16, driver #13 kept more stable and shorter spacing from the leading car by conducting more intensive acceleration and braking maneuvers. Therefore, the risk effect a^R controlled by driver #13 fluctuated gently around a higher level (mean: 0.24, SD = 0.18). This driving strategy was mainly characterized by RRDM_{13} using high risk equilibrium $M_{13} = 0.63$ and high risk sensitivity $S_{13} = 26.98$. The spacing controlled by both driver #13 (mean: 25.82 m, SD = 6.64 m) and RRDM_{13} (mean: 20.33 m, SD

=7.36 m) was shorter and more stable than that controlled by the IDM (mean: 49.8 m, SD = 13.57 m) and the GM (mean: 19.93 m, SD = 11.22 m).

Consistency in spacing control strategies of the human driver and RRDM was recoverable in other driver cases. The mean value and the SD of spacing controlled by the RRDM and human drivers are shown in Figs. 14 and 15, respectively. We could observe that, in most driver cases, the mean value and SD of spacing controlled by RRDM_j showed the same numerical relationship (compared to the two baseline models) as that controlled by driver # j . Moreover, there was a significant correlation between the spacing controlled by human drivers and RRDM in terms of both mean value and SD at a confidence level of 0.1 %. These results indicate that the spacing control strategy of a human driver could be well reproduced by the RRDM.

5.2.2. B. Compound car-following scenario

Fig. 16 shows the driving process of driver #2 in the compound car-following scenario. RRDM_2 was defined by a parameter vector $\mathbf{P}_2 = [a_2^{\max} = 1.60; a_2^{\min} = -1.11; M_2 = 0.60; S_2 = 15.43]^T$, and its driving style map is shown in Fig. 17. In this scenario, an adjacent car merged in and the spacing between the subjective car and the leading car dropped [Fig. 16(a)]. Both the GM and the IDM applied sudden brakes, whereas the braking maneuver made by the RRDM was relatively smoother [Fig. 16(c)]. To various extents, the smoother brake maneuvers around the merging events could as well be observed in the RRDM of other human drivers.

6. Discussion

Trained by real-world human driving data, RRDM could realize longitudinal control in pure and compound car-following tasks where the merge of the adjacent car is considered. Under this section, we will discuss the performance and potential applications of the RRDM based on the results of the simulation.

6.1. Explicit description of driver features

Our expectation for autonomous driving system is that it should make ICVs behave like excellent human drivers or even better. One step prior to learning about the features of a human driver is to quantify the driving style, which we expect to be intuitive and readable, in contrast to

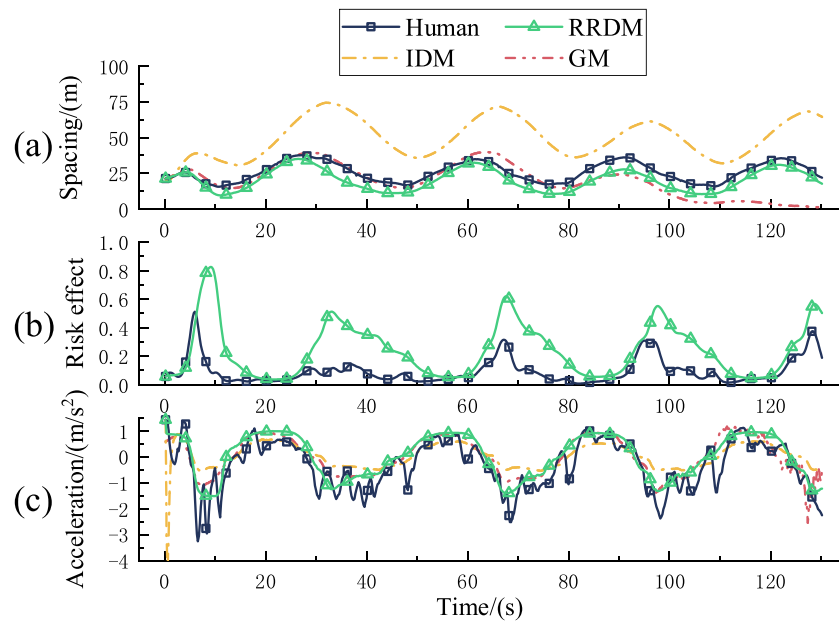


Fig. 12. Driving process of driver #13 in a pure car-following scenario.

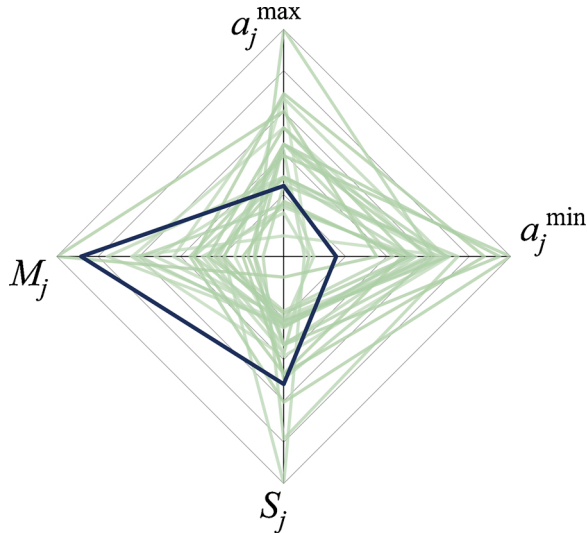


Fig. 13. Style map of driver #13.

qualitatively defining it, which is usually vague and cannot produce access to explicit parameter tuning. The RRDM parameters, in retrospect, revealed four driving features of human drivers. As such, we could directly read the difference among drivers on the basis of the parameters of their RRDM. For example, compared to driver #16 ($M_{16} = 0.52$), driver #13 ($M_{13} = 0.63$) exhibited higher risk-level tolerance, which implies that he/she may follow the leading car more closely; this is sometimes considered an aggressive driving behavior. But simultaneously, driver #13 ($S_{13} = 26.98$) was more sensitive to the driving risk and reacted more actively than driver #16 ($S_{16} = 19.32$) with a change in the driving risk. In essence, it is hard to simply define whether or not driver #13 is an aggressive driver, as is often the case with other drivers. Such a dilemma is always observable when model designers individualize the control model by classification.

From a more general perspective, we could observe from Fig. 8 that only two of the four parameters displayed significant correlations with each other, which means that we can extract at least three independent driver characteristics. With more than three degrees of freedom in the

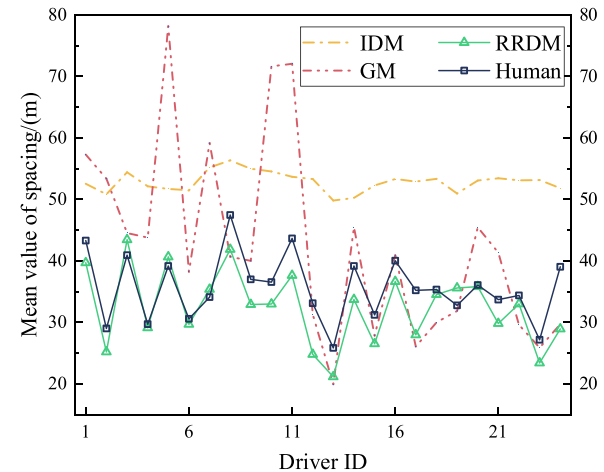


Fig. 14. Mean spacing controlled by a human driver, RRDM, GM, and IDM in all driver cases.

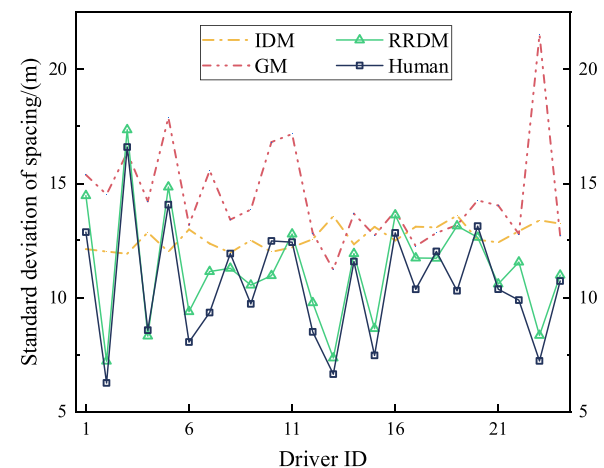


Fig. 15. SD of spacing controlled by a human driver, RRDM, GM, and IDM in all driver cases.

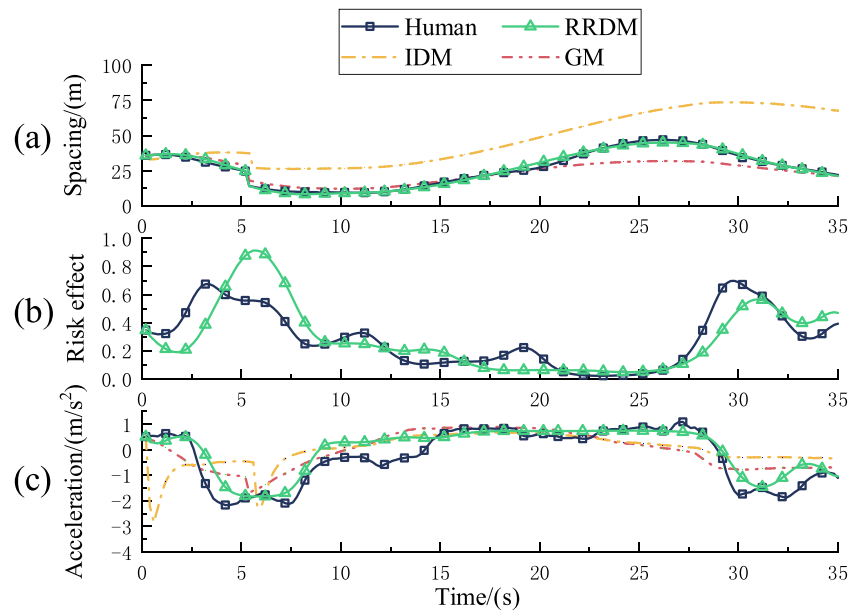


Fig. 16. Driving process of driver #2 in a compound car-following scenario.

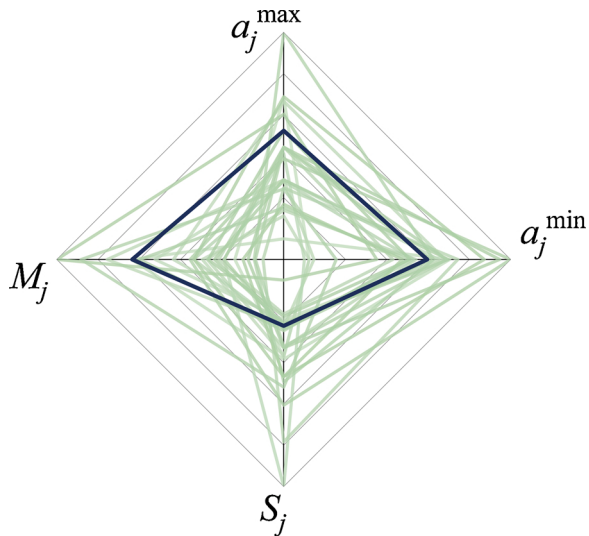


Fig. 17. Style map of driver #2.

driving style, it becomes almost impossible to well classify the driving style using a single-dimensional criterion.

Such identification is possible with the RRDM, explicitly, by extraction of the parameter vector from the driving data of the human driver. Moreover, this parameter vector directly revealed four driving features of human drivers and, from a numerical perspective, enhanced our understanding of how a human driver responds to driving risks. Triggered by the parameter vector, we could look forward to future applications of RRDM that include the numerical and intuitive analyses of excellent human drivers. By learning the risk-response strategy of excellent drivers, we ascertain that we can realize an understandable and human-like driver model to serve autonomous driving.

6.2. Replication of human driving maneuvers

Longitudinal information has been most frequently employed as input for driver models, which are designed for a car-following task. It is obvious in Figs. 10 and 12 that both the GM and the IDM could handle

pure car-following well, which indicates that single-dimensional information is sufficient for such scenario.

However, models that utilize single-dimensional information produced an unsatisfactory performance after encountering cut-in events, which are observed frequently in real-world car-following. Apparently, in Fig. 16(a), for the vehicle controlled by the IDM and GM, merging of an adjacent car could be treated as a drop of spacing from the leading car; hence, both models had to apply sudden brakes. Nevertheless, a few seconds before the merging, the human driver had already started to brake and tried to maintain a proper gap gradually. This response indicates that, from the perspective of human drivers, the car-following task may not be a simple task where only the interaction between the leading car and the subject car is considered. Taking both longitudinal and lateral information into account, the RRDM provides a better interpretation of human maneuvers when dealing with the cut-in of an adjacent car. In fact, during the merging process, the risk increase gradually [Fig. 16(b)], which makes the RRDM give a human-like braking maneuver [Fig. 16(c)].

6.3. Potential extensions

Considering the two experimental scenarios, the RRDM produced a promising performance by learning the risk-response strategy of human drivers. Indeed, such a strategy also exists in traditional driver models like GM or IDM. In the RRDM, the risk is calculated by the risk field model, by considering the effect of lane markers and the longitudinal and lateral position information of surrounding traffic units. In a traditional driver model, however, the longitudinal position of other traffic units could be defined as a risk-related factor. This elicits our intention to further probe into another problem: to further polish the driver model, what are the other risk-related factors that human drivers should consider?

This question brings us to the real-world driving process. As a matter of fact, even in the simplest car-following task, the environmental factors that the driver has to consider are far more than the leading car. Apart from the lane markers that we have considered in the RRDM, traffic signs and lights, road curvature and slope, and the like can all be risk-related factors of human interests. Indeed, a more exact definition of risk creates a better model of human drivers. Therefore, in order to deal with more complex driving tasks, more comprehensive modeling of the traffic risk may be a promising solution. For this point, we have

illustrated the possibility of further developing a traffic risk model in our previous research (Wang et al., 2015).

6.4. Limitations and future work

Firstly, our present work mainly focused on developing a method for modeling the driving strategy of randomly selected human drivers. However, from the perspective of serving autonomous driving, what autonomous driving truly needs is an excellent controller that can deal with different driving situations like a skilled driver. In our future research, we will engage in analyzing the common features in the RRDM of professional human drivers and develop an RRDM-based control method for autonomous driving in real-world scenarios. With this aside, although the risk field model in this paper provides satisfactory performance in both pure and compound car-following scenarios, there remains a need to verify and calibrate its adaptability in more complex cases.

Secondly, from the perspective of driver modeling itself, the between-individual analysis is of great value for understanding the human-related traffic phenomena. The gender, age, and profession, etc. are usually the factors distinguishing human driving behaviors. The RRDM, acting as an explicit driving strategy interpreter, provides a potential tool to analyze the difference in driving behavior between purposively controlled groups. Nevertheless, statistical analysis is currently not possible considering the limited tested participants involved in this work. A wider range of data collection is currently undergoing, and, therefore, such work will be covered in our future research with an enriched dataset.

7. Conclusions

In this paper, we presented a paradigm to elucidate the human driving strategy in analyzing how humans respond to surrounding risks during a driving process. We abstracted the RRDM from real-world driving data in order to formulate a relationship between environmental risks and the driving maneuvers of human drivers. By applying intuitive model parameters, the RRDM could directly reveal the driving features of a specific human driver, learning from his/her driving data. We verified the performance of the RRDM in longitudinal control in both pure and compound car-following scenarios. The simulation results demonstrated that even though our current implementation still limits the control problem in the longitudinal dimension, and indeed could be extended laterally in future studies, the RRDM could produce a more human-like performance compared with traditional single-dimensional models.

CRediT authorship contribution statement

Xiaocong Zhao: Conceptualization, Methodology, Software, Investigation, Visualization, Writing - original draft, Writing - review & editing. **Ren He:** Supervision, Data curation. **Jianqiang Wang:** Resources, Validation, Funding acquisition.

Declaration of Competing Interest

The authors declare that they have no known competing financial interests or personal relationships that could have appeared to influence the work reported in this paper.

Acknowledgments

This work was supported by the National Science Fund for Distinguished Young Scholars (51625503), the National Natural Science Foundation of China, the Major Project (61790561), Postgraduate Research & Practice Innovation Program of Jiangsu Province (SJKY19_2537). We appreciate Dr. Xunjia Zheng for his valuable

suggestions and discussion.

References

- Benderius, O., 2012. Driver Modeling: Data Collection, Model Analysis, and Optimization. Chalmers University of Technology.
- Bojarski, M., Del Testa, D., Dworakowski, D., Firner, B., Flepp, B., Goyal, P., Jackel, L.D., Monfort, M., Muller, U., Zhang, J., Zhang, X., Zhao, J., Zieba, K., 2016. End to end learning for self-driving Cars. *ArXiv160407316 Cs.*
- Cao, B., 2020. A car-following dynamic model with headway memory and evolution trend. *Phys. Stat. Mech. Its Appl.* 539, 122903 <https://doi.org/10.1016/j.physa.2019.122903>.
- Chakraborty, P., Kikuchi, S., 1999. Evaluation of the General Motors based car-following models and a proposed fuzzy inference model. *Transp. Res. Part C Emerg. Technol.* 7 (4), 209–235. [https://doi.org/10.1016/S0968-090X\(99\)00020-0](https://doi.org/10.1016/S0968-090X(99)00020-0).
- Constantinescu, Z., Marinou, C., Vladou, M., 2010. Driving style analysis using data mining techniques. *Int. J. Comput. Commun. CONTROL* 5 (5), 654–663. <https://doi.org/10.15837/ijcc.2010.5.2221>.
- Fu, R., Li, Z., Sun, Q., Wang, C., 2019. Human-like car-following model for autonomous vehicles considering the cut-in behavior of other vehicles in mixed traffic. *Accid. Anal. Prev.* 132, 105260 <https://doi.org/10.1016/j.aap.2019.105260>.
- Goodall, N.J., Lan, C.-L., 2020. Car-Following characteristics of adaptive cruise control from empirical data. *J. Transp. Eng. Part Syst.* 146 (9), 04020097 <https://doi.org/10.1061/JTEPBS.0000427>.
- Gu, Y., Hashimoto, Y., Hsu, L.-T., Iryo-Asano, M., Kamijo, S., 2017. Human-Like motion planning model for driving in signalized intersections. *IATSS Res.* 41 (3), 129–139. <https://doi.org/10.1016/j.iatsr.2016.11.002>.
- Hecker, S., Dai, D., Van Gool, L., 2019. Learning accurate, comfortable and human-like driving. *ArXiv190310995 Cs.*
- Kesting, A., Treiber, M., Helbing, D., 2010. Enhanced intelligent driver model to access the impact of driving strategies on traffic capacity. *Philos. Trans. R. Soc. Math. Phys. Eng. Sci.* 368 (1928), 4585–4605. <https://doi.org/10.1098/rsta.2010.0084>.
- Kuderer, M., Gulati, S., Burgard, W., 2015. Learning driving styles for autonomous vehicles from demonstration. 2015 IEEE International Conference on Robotics and Automation (ICRA). Presented at the 2015 IEEE International Conference on Robotics and Automation (ICRA) 2641–2646. <https://doi.org/10.1109/ICRA.2015.7139555>.
- Li, Z., Li, W., Xu, S., Qian, Y., 2015. Stability analysis of an extended intelligent driver model and its simulations under open boundary condition. *Phys. Stat. Mech. Its Appl.* 419, 526–536. <https://doi.org/10.1016/j.physa.2014.10.063>.
- Liu, K., Gong, J., Kurt, A., Chen, H., Ozguner, U., 2017. A model predictive-based approach for longitudinal control in autonomous driving with lateral interruptions. 2017 IEEE Intelligent Vehicles Symposium (IV). Presented at the 2017 IEEE Intelligent Vehicles Symposium (IV) 359–364. <https://doi.org/10.1109/IVS.2017.7995745>.
- Liu, X., Shen, D., Lai, L., Le Vine, S., 2020. Optimizing the safety-efficiency balancing of automated vehicle car-following. *Accid. Anal. Prev.* 136, 105435 <https://doi.org/10.1016/j.aap.2020.105435>.
- Macadam, C.C., 2003. Understanding and modeling the human driver. *Veh. Syst. Dyn.* 40 (1–3), 101–134. <https://doi.org/10.1076/vsed.40.1.101.15875>.
- Marina Martinez, C., Heucke, M., Wang, F.-Y., Gao, B., Cao, D., 2018. Driving style recognition for intelligent vehicle control and advanced driver assistance: a survey. *IEEE Trans. Intell. Transp. Syst.* 19 (3), 666–676. <https://doi.org/10.1109/TITS.2017.2706978>.
- Marzbanrad, J., Moghaddam, I.T., 2016. Self-Tuning control algorithm design for vehicle adaptive cruise control system through real-time estimation of vehicle parameters and road grade. *Veh. Syst. Dyn.* 54 (9), 1291–1316. <https://doi.org/10.1080/00423114.2016.1199886>.
- McCall, J.C., Trivedi, M.M., 2007. Driver behavior and situation aware brake assistance for intelligent vehicles. *Proc. IEEE* 95 (2), 374–387. <https://doi.org/10.1109/JPROC.2006.888388>.
- Milanés, V., Shladover, S.E., 2016. Handling cut-in vehicles in strings of cooperative adaptive cruise control vehicles. *J. Intell. Transp. Syst.* 20 (2), 178–191. <https://doi.org/10.1080/15472450.2015.1016023>.
- Ni, D., Leonard, J.D., Jia, C., Wang, J., 2015. Vehicle longitudinal control and traffic stream modeling. *Int. J. Transp. Sci. Technol.* 50 (3), 1016–1031. <https://doi.org/10.1287/trsc.2015.0614>.
- Pathak, S., Bag, S., Nadkarni, V., 2019. A generalised method for adaptive longitudinal control using reinforcement learning. In: Strand, M., Dillmann, R., Menegatti, E., Ghidoni, S. (Eds.), Intelligent Autonomous Systems 15, Advances in Intelligent Systems and Computing. Springer International Publishing, Cham, pp. 464–479. https://doi.org/10.1007/978-3-030-01370-7_37.
- Rahman, M.M., Strawderman, L., Lesch, M.F., Horrey, W.J., Babinski-Reeves, K., Garrison, T., 2018. Modelling driver acceptance of driver support systems. *Accid. Anal. Prev.* 121, 134–147. <https://doi.org/10.1016/j.aap.2018.08.028>.
- Treiber, M., Hennecke, A., Helbing, D., 2000. Congested traffic states in empirical observations and microscopic simulations. *Phys. Rev. E* 62 (2), 1805–1824. <https://doi.org/10.1103/PhysRevE.62.1805>.
- Wang, J., Zhang, L., Zhang, D., Li, K., 2013. An adaptive longitudinal driving assistance system based on driver characteristics. *IEEE trans. Intell. Transp. Syst.* 14 (1), 1–12. <https://doi.org/10.1109/TITS.2012.2205143>.
- Wang, J., Wu, J., Li, Y., Li, K., 2014. The concept and modeling of driving safety field based on driver-vehicle-road interactions. 17th International IEEE Conference on Intelligent Transportation Systems (ITSC). Presented at the 17th International IEEE

- Conference on Intelligent Transportation Systems (ITSC) 974–981. <https://doi.org/10.1109/ITSC.2014.6957815>.
- Wang, J., Wu, J., Li, Y., 2015. The driving safety field based on driver–vehicle–road interactions. *IEEE trans. Intell. Transp. Syst.* 16 (4), 2203–2214. <https://doi.org/10.1109/TITS.2015.2401837>.
- Wang, J., Wu, J., Zheng, X., Ni, D., Li, K., 2016. Driving safety field theory modeling and its application in pre-collision warning system. *Transp. Res. Part C Emerg. Technol.* 72, 306–324. <https://doi.org/10.1016/j.trc.2016.10.003>.
- Wang, D., Tan, D., Liu, L., 2018. Particle swarm optimization algorithm: an overview. *Soft comput.* 22 (2), 387–408. <https://doi.org/10.1007/s00500-016-2474-6>.
- Wilson, R.E., 2008. Mechanisms for spatio-temporal pattern formation in highway traffic models. *Philos. Trans. R. Soc. Math. Phys. Eng. Sci.* 366 (1872), 2017–2032. <https://doi.org/10.1098/rsta.2008.0018>.
- Xu, L., Hu, J., Jiang, H., Meng, W., 2015. Establishing style-oriented driver models by imitating human driving behaviors. *IEEE trans. Intell. Transp. Syst.* 16 (5), 2522–2530. <https://doi.org/10.1109/TITS.2015.2409870>.
- Zhu, B., Jiang, Y., Zhao, J., He, R., Bian, N., Deng, W., 2019. Typical-driving-style-oriented personalized adaptive cruise control design based on human driving data. *Transp. Res. Part C Emerg. Technol.* 100, 274–288. <https://doi.org/10.1016/j.trc.2019.01.025>.